Materials and Design 196 (2020) 109107

Contents lists available at ScienceDirect

Materials and Design

journal homepage: www.elsevier.com/locate/matdes

Size effect on the shear damage under low stress triaxiality in micro-scaled plastic deformation of metallic materials

Jilai Wang [a,b,c], Chuanzheng Li [a,b], Yi Wan [a,c], Chengpeng Zhang [a,c,**], Jiaqi Ran [d], M.W. Fu [e,*]

[a] Key Laboratory of High Efficiency and Clean Mechanical Manufacture of Ministry of Education, School of Mechanical Engineering, Shandong University, Jinan, Shandong 250061, China
[b] Shenzhen Research Institute, Shandong University, Shenzhen, 518057, China
[c] National Demonstration Center for Experimental Mechanical Engineering Education, Shandong University, Jinan, Shandong, 250061, China
[d] College of Mechatronics and Control Engineering, Shenzhen University, Shenzhen, China
[e] Department of Mechanical Engineering, The Hong Kong Polytechnic University, Hung Hom, Kowloon, Hong Kong

HIGHLIGHTS

- A new micro-scaled model is proposed for fracture under low stress triaxiality.
- Shear damage and its size effect is considered in a phenomenological way.
- Void and shear damage can be quantified by two independent parameters.
- With the increase of grain size, fracture becomes more shear-dominated.

GRAPHICAL ABSTRACT

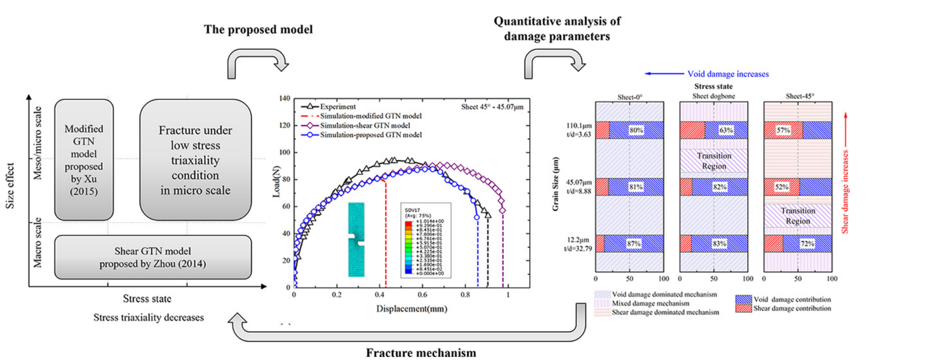

ARTICLE INFO

Article history:
Received 16 July 2020
Received in revised form 18 August 2020
Accepted 27 August 2020
Available online 2 September 2020

Keywords:
Micro-scaled deformation
Size effect
Shear damage
GTN model
Fracture mechanism

ABSTRACT

Micro-forming is one of the major micro-manufacturing methods with promising application potentials, in which the damage response and fracture behavior need to be insightfully addressed. Among all the damage criteria to predict fracture, GTN model is a widely-used one and able to predict void-dominated fracture in micro-scale deformation. However, it is not very applicable under low stress triaxiality and shear-dominated condition. An in-depth understanding of shear damage and its potential size effect are crucial to explore the micro-scaled damage and fracture mechanisms. This research characterizes the size effect on flow stress via employing a combined constitutive model, and an approach for applying a phenomenological shear damage evolution law to the GTN-Thomason model via considering the size effect is developed. The prediction of micro-scaled fracture in a wide stress triaxiality range is thus enabled. Through simulation and experiment, the proposed model is validated and verified. In addition, stress state parameters including stress triaxiality, Lode parameter, and weight function, are also discussed, and the two damage parameters are analyzed quantificationally to reveal different fracture mechanisms occurring in different stress states and grain sizes. The research thus facilitates the physical insight and in-depth understanding of the size effect on damage evolution and fracture formation in micro-scaled plastic deformation of materials.

* Corresponding author.
** Corresponding author at: Key Laboratory of High Efficiency and Clean Mechanical Manufacture of Ministry of Education, School of Mechanical Engineering, Shandong University, Jinan, Shandong 250061, China.
E-mail addresses: zhangchengpeng@sdu.edu.cn (C. Zhang), mmmwfu@polyu.edu.hk (M.W. Fu).

https://doi.org/10.1016/j.matdes.2020.109107

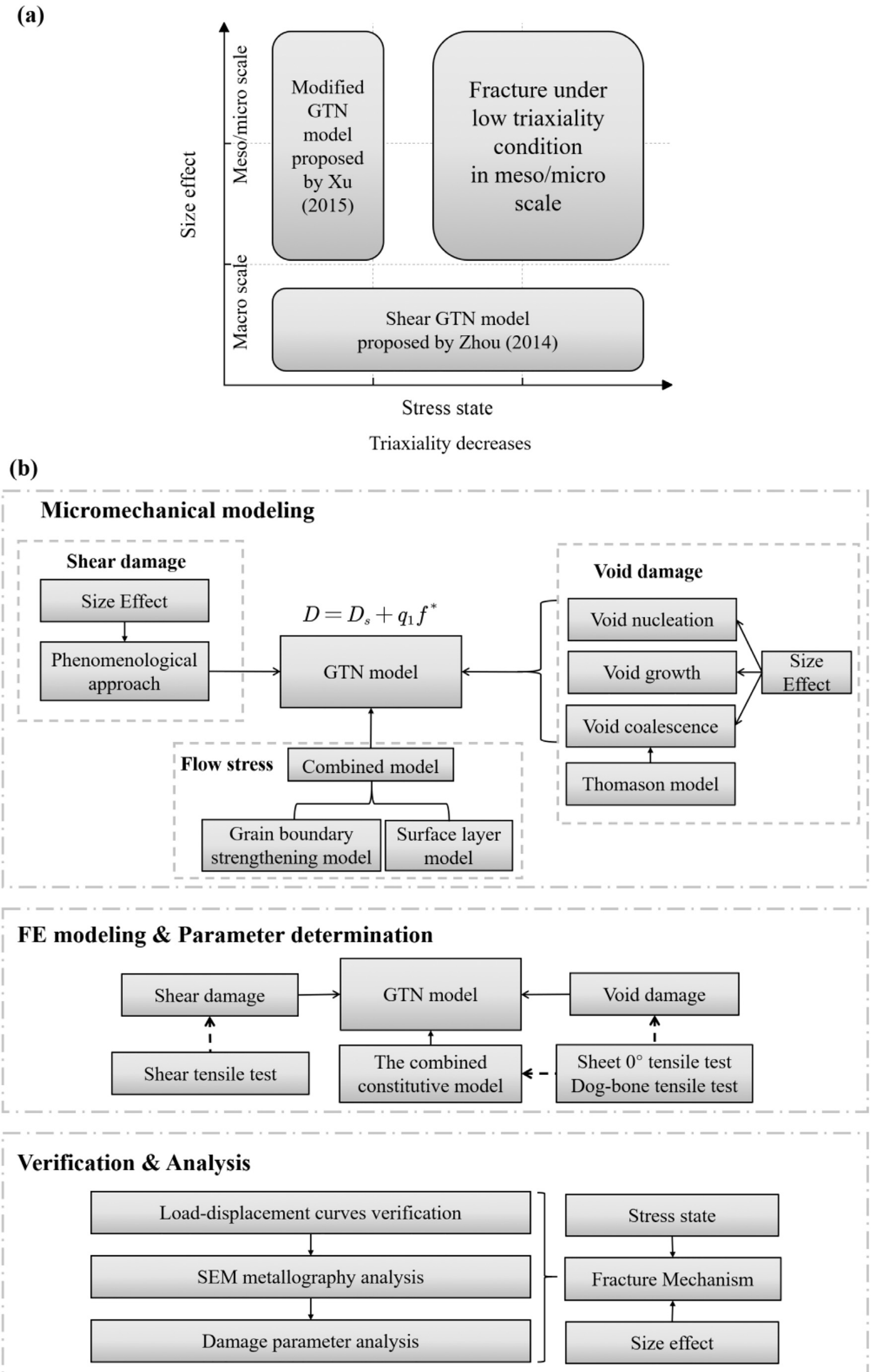

Fig. 1. Research procedure.

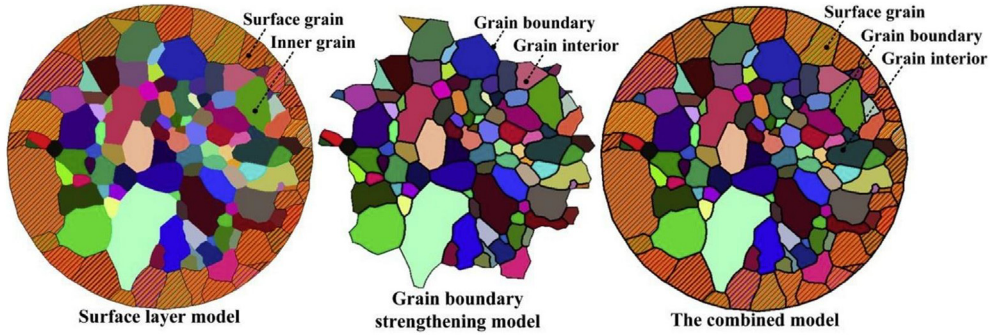

Fig. 2. The material composition in the combined model [24].

1. Introduction

With the growing demand for product miniaturization, micro-forming technology has been widely studied and developed for its advantages of low production cost, high productivity, and good product property [1]. However, due to the size effect (SE) on flow stress [2], friction behavior [3] and microstructure evolution [4], macroscopic laws become not fully valid or inapplicable for the deformation of materials in microscopic scale, and the traditional ductile fracture criteria (DFC) cannot well predict the ductile fracture (DF) in micro-scaled deformation of metallic material, which hinders the wide applications of micro-forming technology [5]. Thus, understanding of SE and developing of DFC applicable in micro-scale are crucial in development and application of micro-forming technology.

There has been a long history of research on the macro-scale DF of metallic materials and there are many DFCs applicable [6]. Among these DFCs, the GTN model is a widely-used classical micromechanical model with a sound physical basis. It was originally introduced by Gurson [7] and subsequently modified [8], in which a representative volume element (RVE) containing a micro-void with the simplified shape is used for description of the mechanical behavior of the porous material. Many experiments and studies have also been carried out to explore the applicability of GTN model and develop it further with consideration of different factors. As a complementary criterion for void coalescence, the Thomason model [9] assumes that the void coalescence occurs when there is a localized plastic deformation in the inter-void ligaments. It could be used in conjunction with the GTN model, which is proven to be a feasible way for prediction of DF of materials [10].

Sketching a bit of the long research history and various DFC in macro scale, micro-scaled DF has been just started to be focused, but there is a lack of in-depth understanding of damage, fracture and failure. Peng et al. [11] proposed a surface layer constitutive model to describe the size effect on flow stress of CuZn36 sheets of different thickness based on the uniaxial tensile experiments. Vollertsen and Hu [12] conducted the pneumatic bulge tests using the aluminum foil and observed quite irregular local strain distributions and random fracture in the deformation zone. Fu and Chan [13] conducted the tensile test of copper foils with various thicknesses and microstructures. Experimental results suggested that as the thickness/grain number ratio becomes smaller, the number of dimples is decreased gradually, and material formability is decreased. Furushima et al. [14] found that the fracture strain and dimple of pure copper metal foil are decreased with the foil thickness. Therefore, the macroscopic DFCs cannot be used to predict the fracture of metallic sheet during micro-forming without an extensive investigation of the mechanism and influencing factors of size effect [15]. To predict microscopic DF and obtain the forming limit diagram (FLD) of Cu-FRHC sheets, Xu et al. [16] considered the SE on void nucleation and coalescence behavior using the specimens with different sizes of grain and sheet thickness, and a modified GTN model considering the SE was obtained and proved to be capable of characterizing the influence of SE on forming limit of metallic sheet.

However, Xu et al. [16] found that the FLD obtained by the modified GTN model tends to be higher under the low stress triaxiality conditions. The reason may be the fact that the void coalescence induced by the shear loading component is not considered, and therefore the fracture in shear-dominated condition cannot be predicted accurately. In the past decades, on the other hand, many studies have been focused on addressing this issue in macro-scale. Xue [17] and Nahshon and Hutchinson [18] regarded the void volume fraction as a combined damage variable contributed from both void damage and shear damage, which improves the prediction accuracy. Nielsen and Tvergaard [19] adjusted the evolution law of shear damage when the stress triaxiality is relatively high. Achouri et al. [20] introduced a novel calibration procedure for calibrating the Nahshon and Hutchinson's modified model and conducted the corresponding finite element (FE) simulation for HSLA steel. The simulation results were in good agreement with different experiments, and in-situ tests showed the difference of physical mechanisms between ductile damage under tensile and shear load. Zhou et al. [21] introduced a novel approach to using two independent damage parameters to represent the volume damage and shear damage respectively and integrated the continuum damage mechanics (CDM) concept of Lemaitre [22] with the GTN model. The modified shear damage GTN model was successfully used to predict the DF behavior of Zircaloy-4.

Furthermore, the relationship between stress state and DF has also been much concerned in micro-scale recently. Wang et al. [23] carried out tests of pure copper with diverse geometric dimensions and grain sizes and numerical simulations to analyze the effects of stress condition

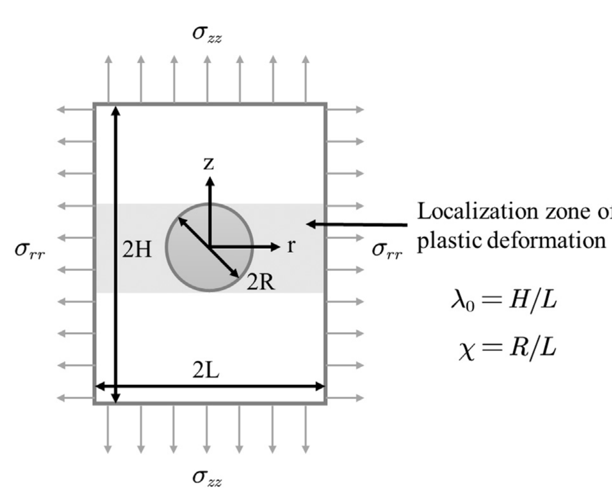

Fig. 3. The Thomason model of spherical voids in cylindrical cells.

and SE on DF. Li et al. [24] conducted a collection of tests of micro-scaled copper specimens and established the interactive influences of stress triaxiality and grain size on the DF. It was found that the larger *d* or the higher stress state would lead to the larger fracture strain of metallic sheets.

Although with the efforts of many researchers, the GTN model has been developed to be more accurate in predicting micro-scale fracture, when the micro-scale DF occurs under low stress triaxiality and is mainly induced by shear damage, the modified GTN model is inaccurate without consideration of shear damage and its SE, which is a critical issue to be solved. Furthermore, there is still a lack of more systematic research on exploring SE on damage response and failure mechanism in micro-scale. This research thus aims at establishing a DFC to predict DF under low stress triaxiality based on analysis and understanding of the micro-scaled damage response and fracture mechanism. In tandem with this, a series of tensile tests of metallic specimens with diverse geometrical dimensions and microstructural grain sizes were carried out, and a combined DFC was developed via considering SE on flow stress, volumetric damage and shear damage. The experimental results were compared with the corresponding FE simulations in such a way to not only understand the two damage mechanisms, but also reveal how the SE affects the damage evolution quantificationally. This study eventually seeks to provide a well-rounded exploration of the failure mechanism of metallic sheets affected by SE and stress state in micro-scale.

2. Research methodology

2.1. Research procedure

As illustrated in Fig. 1, the procedure of this study is summarized. The micro-scaled GTN model proposed by Xu et al. [16] can predict void-dominated fracture with consideration of SE on void nucleation and coalescence, while the shear damage model introduced by Zhou et al. [21] is applicable when the stress triaxiality is low in macro scale. To predict micro-scaled DF under low stress triaxiality condition, some modifications of GTN-Thomason model are employed to characterize the SE on the volumetric damage firstly. The combined model of the surface layer model (SLM) and the grain boundary strengthening model (GBSM) is introduced to characterize the SE via the developed constitutive equation. Finally, considering the fact that the shear damage has an influence on damage accumulation under low stress triaxiality, the GTN model is combined with shear damage model and the SE of shear damage is further considered. The final combined GTN model is used in FE simulations using ABAQUS subroutine VUMAT.

The tensile tests of dog-bone sheets with various microstructures were used to determine the material constants in the constitutive model; while tension tests with high and low stress triaxiality were employed to determine the void and shear damage constants. The simulation results of the remaining tensile tests with various grain sizes are compared with the experimental ones to verify the proposed model. Furthermore, the qualitative scanning electron microscope (SEM) metallography and quantitative damage parameters are also analyzed to discuss the combined interaction of stress condition and the SE on damage and fracture mechanisms.

2.2. Modeling process

2.2.1. The combined constitutive model of flow stress considering size effect

There is a certain dependence of flow stress on the material microstructures and feature sizes in micro-forming process, which must be carefully modeled in micro scaled DFC. To characterize the influence of SE on flow stress, the widely used SLM proposed by Lai et al. [25] and Peng et al. [26] divides the stress of basis material into a surface component and an inner component:

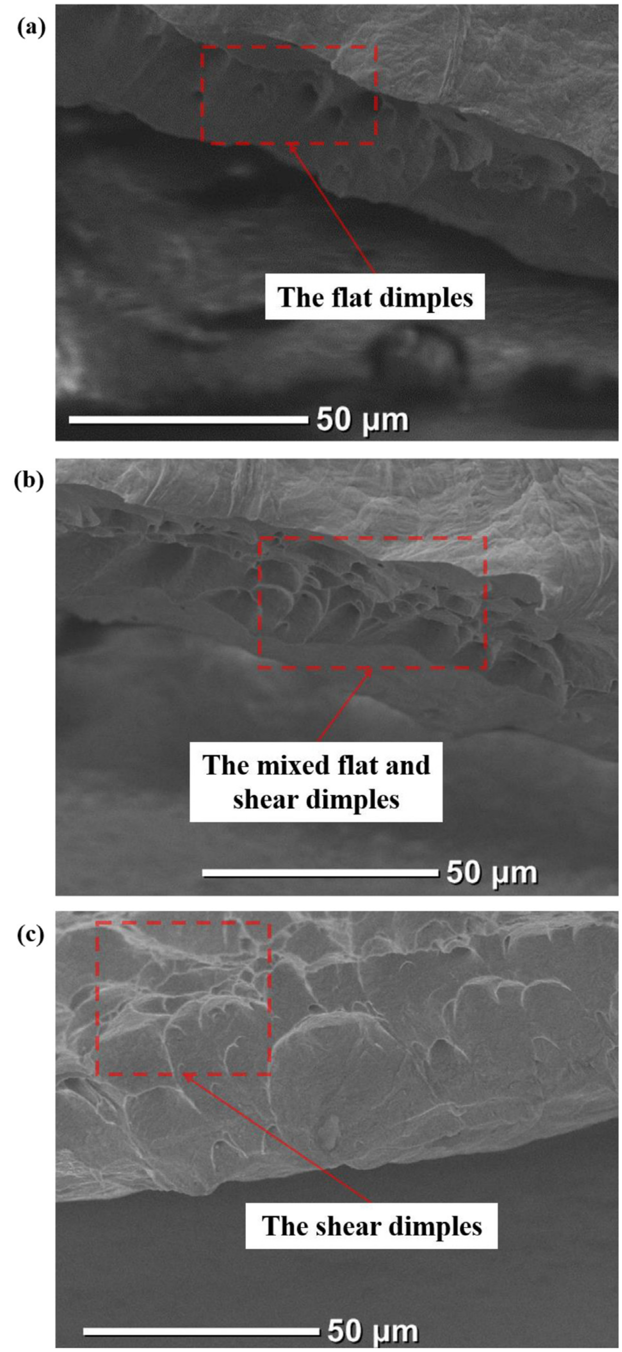

Fig. 4. Different types of dimples in SEM fractography of metallic sheets in the combined tensile-shear sheet-45° test.

$$\begin{cases} \overline{\sigma} = \eta\overline{\sigma}_s + (1-\eta)\overline{\sigma}_i \\ \eta = \dfrac{N_s}{N} \end{cases} \tag{1}$$

where N is the total figure for grains. $\overline{\sigma}_s$ and N_s are the stress and the figure for grains in the surface component, separately, while $\overline{\sigma}_i$ and N_i are them of the internal grains. According to Peng et al. [26], the crystal plastic theory can be employed to represent the stress of surface grain (SG). Furthermore, the strength of the inner grain can be formulated as the grain boundary (GB) component and grain interior (GI) component according to the grain boundary strengthening model (GBSM)

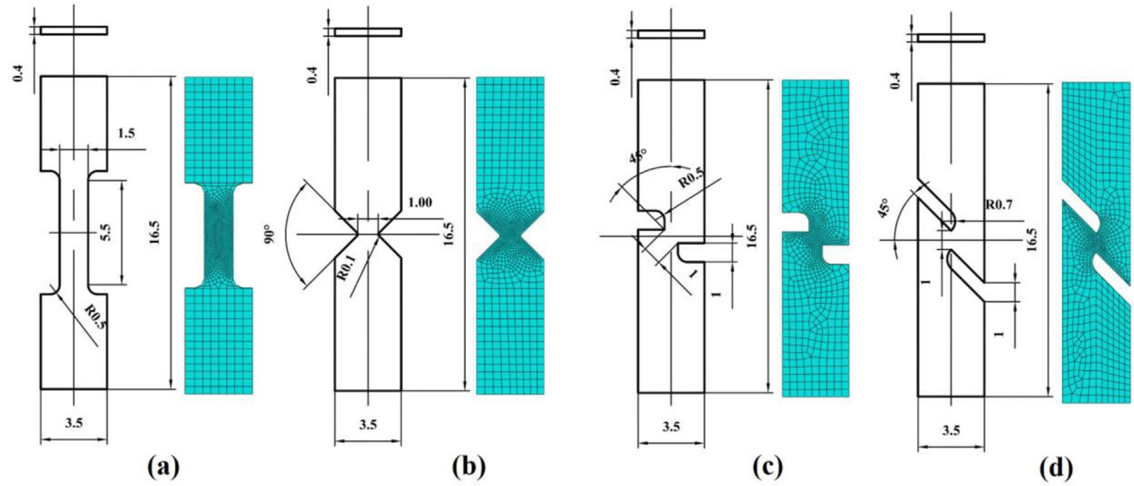

Fig. 5. The geometrical sizes and typical meshes of different specimens. (a) Dog-bone specimen, (b) Sheet-0° specimen, (c) Sheet-45° specimen, and (d) Sheet-90° specimen. (Dimensions in mm).

[27]. Hence, the material constitutive equation described by this combined model consists of the SG, GB and GI parts, as shown in Fig. 2:

$$\begin{cases} \overline{\sigma} = f_{\mathrm{surf}} m\tau_R(\varepsilon) + f_{gb}\left(\sigma_y^{gb} + k_{gb}p + h_{gb}\varepsilon^{n_{gb}}\right) \\ \quad + f_{gi}\left(\sigma_y^{\infty(gi)} + kd^{-1/2} + \left(h_{gi}^{\infty} + ad^{-1/2}\right)\varepsilon^{n_{gi}}\right) \\ 1 = f_{\mathrm{suff}} + f_{gb} + f_{gi} \end{cases} \tag{2}$$

where f_{suff}, f_{gb} and f_{gi} are the proportions of the SG, GB, and GI, separately. $m$represents the orientation factor of single crystal and τ_R represents the critical resolved stress. σ_y^{gb} is the yield stress of the GB, while k_{gb}, h_{gb} and n_{gb} are all material constants of the GB. n_{gi} is the work hardening exponent of the GI, while $\sigma_y^{\infty(gi)}$, k, h_{gi}^{∞} and a are material parameters of single crystals. In addition, d is the grain size of material and p is the spherical stress in the deformation process. By dividing the contribution of flow stress into these three parts, the characterization of SE on flow stress is enabled.

2.2.2. The micro-scaled GTN-Thomason model considering size effect

The related yield equation and the evolution of voids in the GTN model can be designated as [7,8]:

$$\begin{cases} \phi = \left(\dfrac{q}{\overline{\sigma}_m}\right)^2 + 2q_1 f^* \cosh\left(-\dfrac{3}{2}\dfrac{q_2 p}{\overline{\sigma}_m}\right) - \left(1 + q_1^2 f^{*2}\right) = 0 \\ f^* = \begin{cases} f, & f \le f_c \\ f_c + \dfrac{f_u^* - f_c}{f_f - f_c}(f - f_c), & f > f_c \end{cases} \end{cases} \tag{3}$$

where q is the von Mises stress, and $\overline{\sigma}_m$ is the equivalent stress of the matrix. q_1 and q_2 are two coefficients introduced by Tvergaard and Needleman [8]. The practical void volume fraction f is composed of two components: void growth and nucleation. The evolution pattern of void growth can be obtained by the law of bulk material incompressibility; while the evolution pattern of void nucleation can be represented by a normal distribution controlled by strain, which was suggested by Chu and Needleman [28]. When f reaches the critical

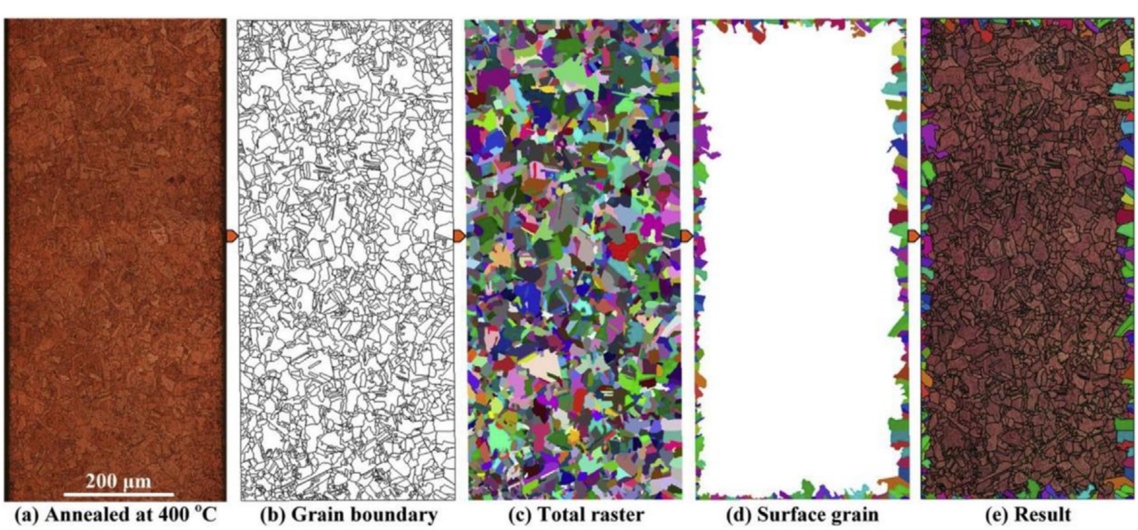

Fig. 6. Schematic graphs to distinguish SG, GB and GI [24] .

Table 1
Area ratios of SG, GB, and GI for different grain sizes.

Grain size (μm)	$f_{surf}(\%)$	$f_{gb}(\%)$	$f_{gi}(\%)$
12.2	10.58	6.9	82.52
45.07	17.88	5.12	77.00
110.1	40.18	2.21	57.61

Table 2
The calibrated parameters of the proposed model.

q_1	q_2	ε_N	S_N	κ	χ_c	$f_f - f_c$	f_n	C	ε_f^s	n
1.5	1	0.3	0.1	1	0.9	0.107	0.032	0.257	0.85	2

value f_c, the effective value f^* is increased rapidly with the acceleration of $\frac{f_u^*-f_c}{f_f-f_c}$, which suggests that void coalescence will occur.

The void coalescence can be further estimated by the Thomason model. As shown in Fig. 3, a cylindrical cell with a spherical void is used as the RVE, in which the stress tensor is axisymmetric and σ_{zz} is greater than σ_{rr}. $\lambda_0 = H/L$is the fraction of the height (H) and the width (L) of the RVE at the beginning, characterizing the dimensional distribution of micro-cavity. $\chi = R/L$ represents the fraction of the diameter of the void to the width of the RVE, which decides whether void coalescence happens. The stress concentration described by the Thomason model is formulated as [29]:

$$\frac{\sigma_{zz}}{\overline{\sigma}_m} = (1-\chi^2)\left[0.1\left(\frac{1}{\chi}-1\right)^2 + 1.2\sqrt{\frac{1}{\chi}}\right] \tag{4}$$

According to Besson [30], the void space ratio χ can be calculated by

$$\chi = \left[\frac{3}{2}f\lambda_0\left(\frac{3}{2}\kappa e_{zz}\right)\right]^{1/3} \tag{5}$$

where e_{zz} represents the major principal strain and κ represents a constant for different materials. When χ approaches 1, the inter-void ligament becomes short enough to form a microcrack, so here $\chi_c = 0.9$ can be used as the critical time of void coalescence [16].

In order to apply the macroscopic feasible GTN-Thomason model to micro-scaled fracture of sheet metal, Xu et al. [16] considered the SE on void nucleation and coalescence behavior using two size-related parameters: grain size d and sheet thickness t. With these two parameters to describe SE on void evolution and some derivation, the modified GTN-Thomason model in micro-scale could be represented as:

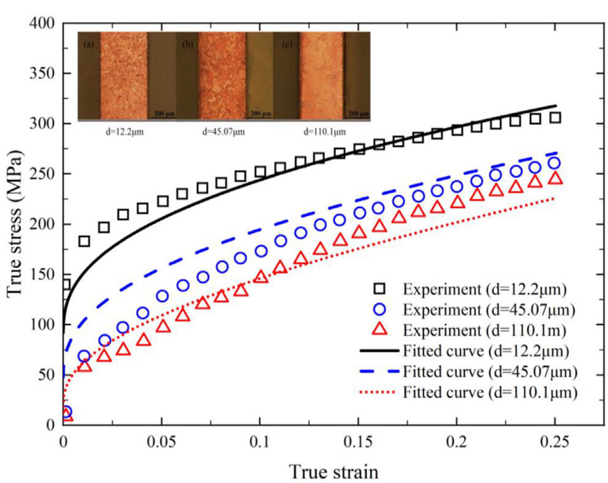

Fig. 7. The fitted stress-strain relationships of the combined model.

$$\begin{cases} \dot{f}_{nucleation} = \dfrac{f_n(1-d/t)}{s_N\sqrt{2\pi}}\ exp\left(-\dfrac{1}{2}\left(\dfrac{\overline{\varepsilon}^p-\varepsilon_N}{s_N}\right)\right)^2 \dot{\overline{\varepsilon}}^p \\ \dot{f}_{growth} = (1-f)\dot{\overline{\varepsilon}}^p \\ \lambda_0 = \dfrac{H}{L} = Cd\rho(\overline{\varepsilon}^p) \\ \rho(\overline{\varepsilon}^p) = \displaystyle\int \frac{\rho_0}{s_N\sqrt{2\pi}}\ exp\left(-\frac{1}{2}\left(\frac{\overline{\varepsilon}^p-\varepsilon_N}{s_N}\right)\right)^2 d\overline{\varepsilon}^p \approx \dfrac{exp\left(\dfrac{4}{s_N\sqrt{2\pi}}\overline{\varepsilon}^p-\varepsilon_N\right)}{1+\ exp\left(\dfrac{4}{s_N\sqrt{2\pi}}\overline{\varepsilon}^p-\varepsilon_N\right)} \end{cases} \tag{6}$$

where f_n, ε_N, S_N, C are all material constants. In this modified GTN model, when the grain size d is increased or the thickness t is decreased, the void nucleation chance becomes smaller with the smaller size-related parameter $(1 - d/t)$, and the thickness of inner layer is also decreased. Therefore, λ_0 is increased and the void coalescence is more likely to occur. With these modifications, the description of SE on void evolution under tensile load is enabled.

2.2.3. The micro-scaled GTN-Thomason model under the low stress triaxiality

The micromechanics of ductile damage is different between tension and shear load [20]. The nucleation and growth of the micro-cavity oriented in loading direction dominates under tensile load, while the elongation and rotation of the micro-cavity dominates under shear load, which could be described by the evolution of flat, shear and mixed dimples as shown in Fig. 4. The macroscopic GTN model to predict DF under low stress triaxiality and shear-dominated conditions proposed by Zhou et al. [21] can be formulated as:

$$\begin{cases} \phi = \left(\dfrac{q}{\overline{\sigma}_m}\right)^2 + 2q_1f^*\ cosh\left(-\dfrac{3}{2}\dfrac{q_2p}{\overline{\sigma}_m}\right) - \left(1+(q_1f^*+D_s)^2 - 2D_s\right) = 0 \\ D = q_1f^* + D_s \end{cases} \tag{7}$$

where D_S is the shear damage parameter and D is the entire damage parameter. When D approaches one, the fracture of metallic material occurs. The shear damage results from the potential contribution of various failure mechanisms, which might be quite complicated. Therefore, a phenomenological method was adopted and it is supposed that the shear damage is induced by the progress of plastic deformation following the formulations below:

$$\begin{cases} D_s = g(\theta)\left(\dfrac{\overline{\varepsilon}^p}{\varepsilon_f^s}\right)^n \\ \dot{D}_s = g(\theta)n\left(\dfrac{\overline{\varepsilon}^p}{\varepsilon_f^s}\right)^{n-1}\dot{\overline{\varepsilon}}^p = g(\theta)n\dfrac{D_s^{\frac{n-1}{n}}}{\varepsilon_f^s}\dot{\overline{\varepsilon}}^p \end{cases} \tag{8}$$

where $\overline{\varepsilon}^p$ is the matrix plastic strain and n represents a softening power index. Since n is larger than one, the softening effect becomes more significant as the metallic material gradually deteriorates during the deformation process. When $\overline{\varepsilon}^p$ is finally increased to effective failure strain under pure shear ε_f^s, D_S reaches to unity and fracture occurs. Furthermore, a coefficient of shear damage is proposed as a weight function about Lode angle θ, to extend the evolution law for an arbitrary stress state. The weight function should be one when the material is under pure shear load and become zero when shear damage is uninvolved,

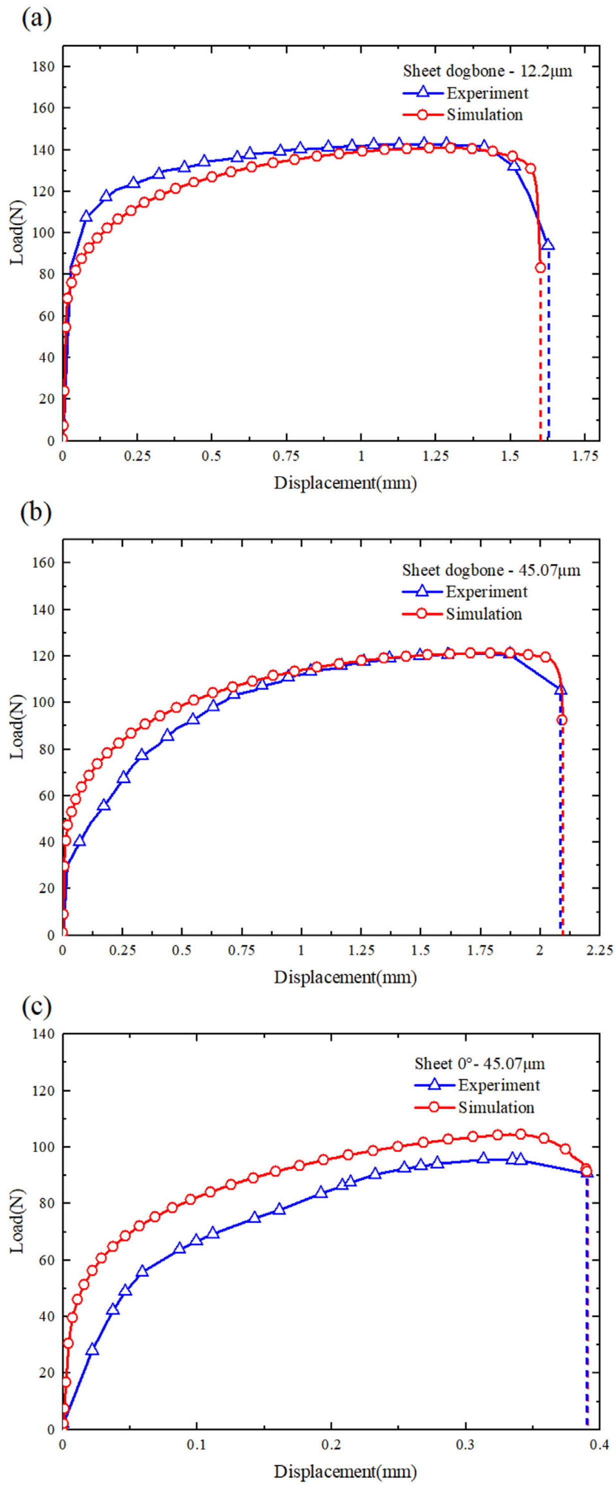

Fig. 8. Load-displacement curves for tensile tests in which void damage is dominated. (a) Sheet dogbone —12.2 μm, (b) Sheet dogbone - 45.07 μm, (c) Sheet 0° - 45.07 μm.

which could be employed as the $g(\theta)$ function for positive stress triaxiality [18]:

$$\begin{cases} g(\theta) = 1 - [\cos(3\theta + \pi/2)]^2 \\ \cos(3\theta + \pi/2) = \dfrac{27J_3}{2q^3} \end{cases} \tag{9}$$

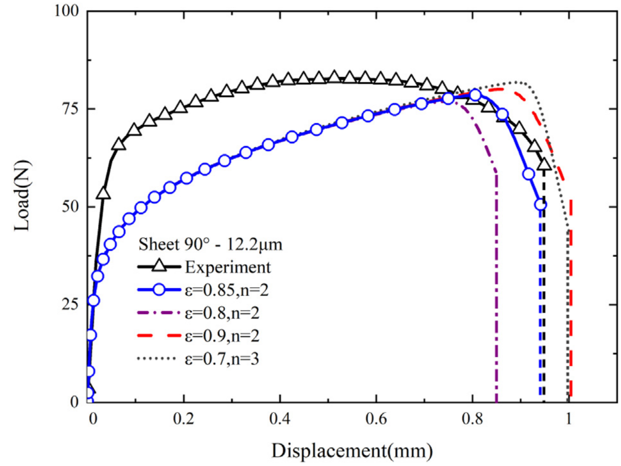

Fig. 9. Calibration of shear damage parameters.

By integrating the micro-scaled GTN-Thomason model introduced by Xu et al. [16] into the shear damage GTN model introduced by Zhou et al. [21], a combined model with consideration of SE and shear damage is obtained, which is applicable for DF not only in shear dominated fracture with the description of shear damage, but also in micro-scaled void-dominant fracture with the description of SE on void damage. Since the shear damage evolution law proposed by Zhou et al. [21] was obtained in a phenomenological way, the SE on the shear damage should be involved and could be described using a size-related parameter $(d/d_0)^{1/2}$:

$$D_s = g(\theta)\left(\frac{d}{d_0}\right)^{\frac{1}{2}}\left(\frac{\overline{\varepsilon}^p}{\varepsilon_f^s}\right)^n \tag{10}$$

where the form of shear damage evolution in Eq.(8) is preserved, and d_0 is the grain size of the shear test used to calibrate shear damage parameters while d is the actual grain size. When d equals to d_0, the size-related parameter is one and no size effect on shear damage is involved. When the grain is coarsened, the size effect on shear damage is intensified because the size-related parameter is larger than one. Thus, the proposed GTN model is summarized in the following equations:

$$\begin{cases} \phi = \left(\dfrac{q}{\overline{\sigma}_m}\right)^2 + 2q_1 f^* \cosh\left(-\dfrac{3}{2}\dfrac{q_2 p}{\overline{\sigma}_m}\right) - \left(1 + (q_1 f^* + D_s)^2 - 2D_s\right) = 0 \\ D = q_1 f^* + D_s \\ \dot{f} = \dot{f}_{growth} + \dot{f}_{nucleation} \\ \chi = \left[\dfrac{3}{2} f \lambda_0 \left(\dfrac{3}{2}\kappa e_{zz}\right)\right]^{\frac{1}{3}} \\ D_s = g(\theta)\left(\dfrac{d}{d_0}\right)^{\frac{1}{2}}\left(\dfrac{\overline{\varepsilon}^p}{\varepsilon_f^s}\right)^n \end{cases} \tag{11}$$

This new model divides damage contributions into two fracture mechanisms: void damage $q_1 f^*$ and shear damage D_S, and they are both extended to micro-scale with the corresponding SE characterized by size-related parameters. When the general damage parameter $q_1 f^* + D_s$ reaches to one, the load capacity fails completely. The model is a combination of the micromechanical interpretation and the phenomenological approach, because it will be reduced to the GTN model when the shear damage is uninvolved and degenerates to the CDM of Lemaitre when only shear load is applied.

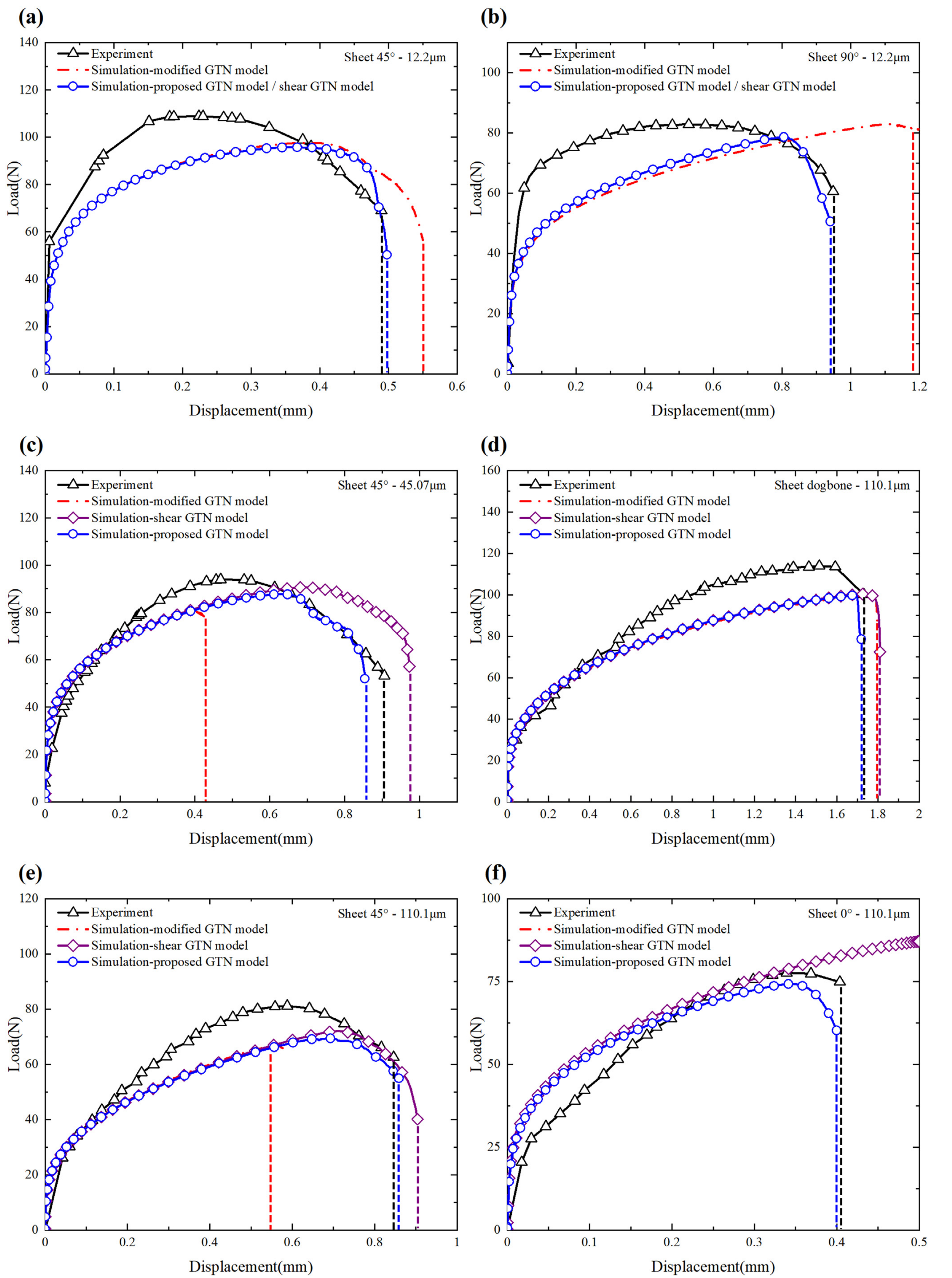

Fig. 10. Experimental and simulation results obtained with different models. (a) Sheet 45° -12.2 μm, (b) Sheet 90° - 12.2 μm, (c) Sheet 45° - 45.07 μm, (d) Sheet dogbone - 110.1 μm, (e) Sheet 45° - 110.1 μm, (f) Sheet 0° - 110.1 μm.

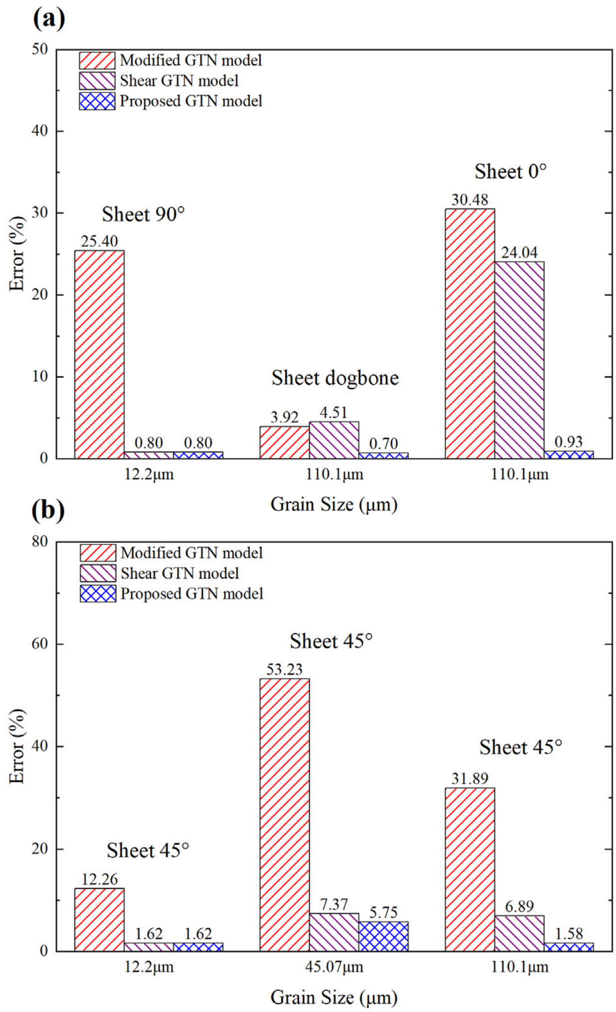

Fig. 11. Prediction error of displacement at fracture using different models.

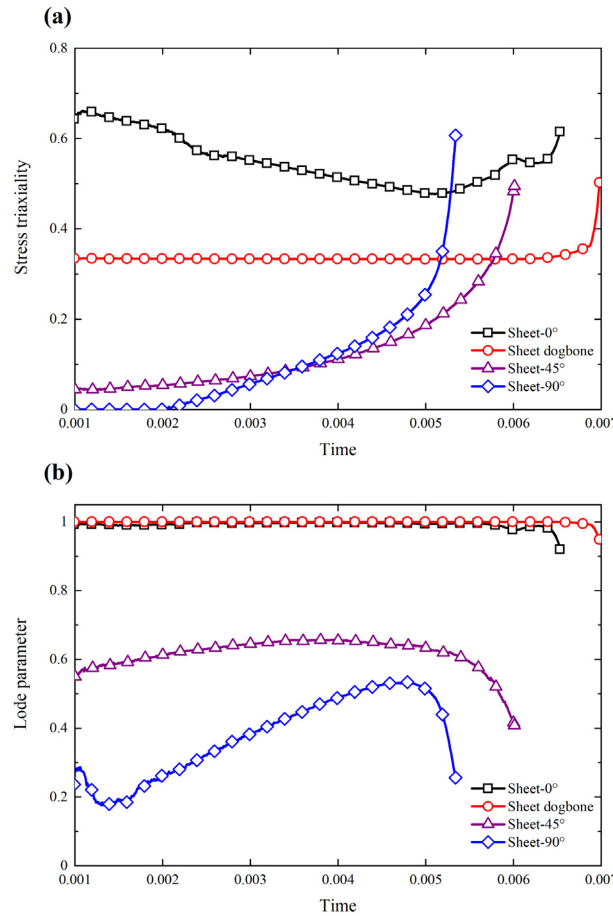

Fig. 12. The evolution of stress state parameters when the grain size is 12.2 μm. (a) Stress triaxiality, (b) Lode parameter.

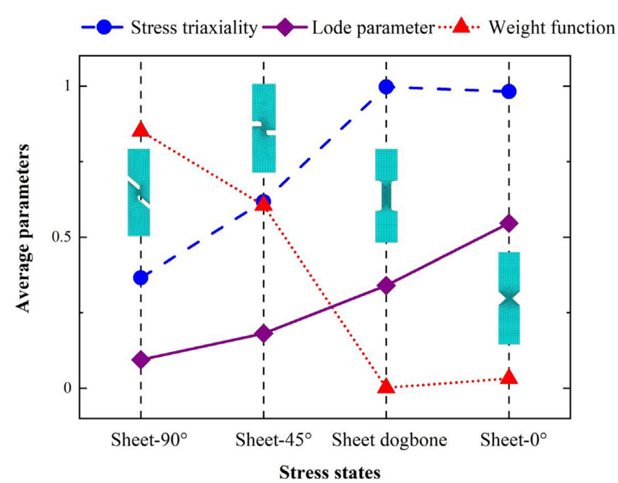

Fig. 13. Average of the parameters in the deformation process.

2.3. Experimental method

A series of micro-scaled tests of pure copper specimens fabricated with diverse geometric configurations and microstructural grain sizes were carried out to realize the SE on shear damage and failure mechanism under tensile, shear and combined tensile-shear loading. Four types of sheet specimens presented in Fig. 5 were annealed at 400, 600 and 750 °C for 1 *h*, respectively, and three individual grain sizes were attained.

2.4. Parameters determination

The proposed model is employed in the FE simulation with the FE software ABAQUS/Explicit with a user subroutine VUMAT. A numerical algorithm of elastic prediction and plastic correcting radial return is implemented into the FE code. The element type is modeled as C3D8R, and the meshing of the sheet specimens are demonstrated in Fig. 5. The parameters of material are calibrated as follows.

The tensile tests could be employed for the calibration of the related parameters in the proposed model. Firstly, the material constitutive relationship in the combined model is obtained. According to Li et al. [24], the fractions of SG, GI and GB could be extracted with ArcMap software via digital image technology (DIT) based on the metallographs of these sheet specimens. The detailed process is illustrated in Fig. 6. With these attained data and the true stress-strain relationships of dog-bone sheets, the combined constitutive relationship can be described as:

$$\begin{cases} \sigma(\varepsilon) = f_{\text{suff}} 551.49\varepsilon^{0.95} + f_{gb}\left(450 + 0.4p + 0.02\varepsilon^{0.9}\right) \\ \quad + f_{gi}\left(-14.15 + 309.87d^{-1/2} + \left(447.9 + 0.01d^{-1/2}\right)\varepsilon^{0.4}\right) \\ 1 = f_{\text{surf}} + f_{gb} + f_{gi} \end{cases} \quad (12)$$

The obtained area proportions of SG, GB, and GI for different d are demonstrated in Table 1, and the fitting curves of stress and strain

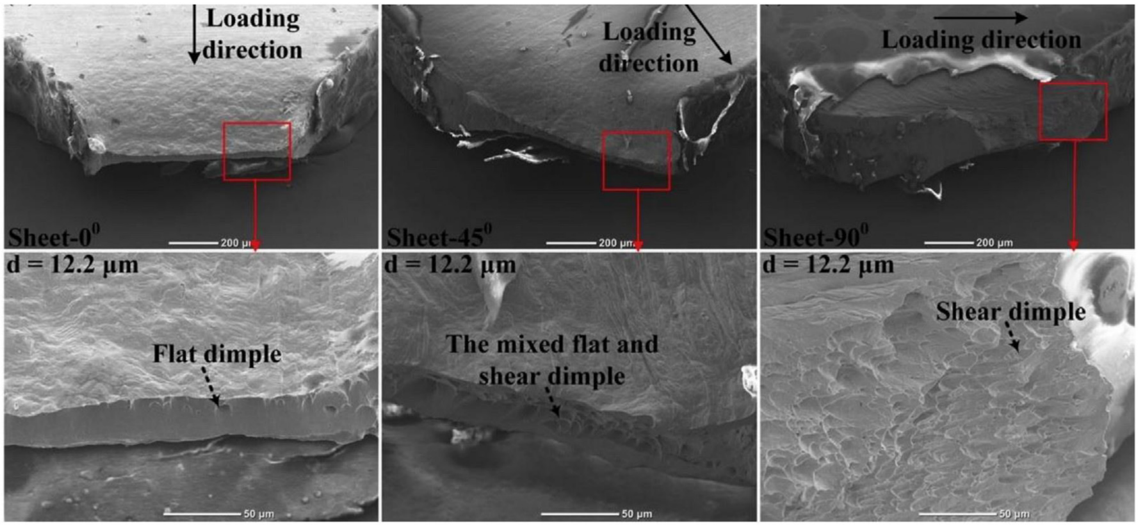

Fig. 14. SEM fractography of sheet specimens with different geometries [24].

relationship are illustrated in Fig. 7. There are great agreements between experimental and calculated curves, and the trend is that for the same sheet thickness, the larger d, the smaller $\sigma(\varepsilon)$.

An inverse approach is adopted to calibrate the damage constants in the proposed model by comparing the numerical and experimental load-displacement relationships. The model calibration strategy mainly consists of two parts. For specimens where fracture is mainly caused by the volumetric damage, the dimple damage constants could be calibrated, while the shear damage constants could be obtained with the shear tension test where the fracture mechanism is shear-dominated.

According to Xu et al. [16], $q_1 = 1.5$, $q_2 = 1$ are commonly used for GTN model. ε_N represents the mean strain of void nucleation and $\varepsilon_N = 0.3$, $S_N = 0.1$ are used for the dog-bone sheet specimens based on the experimental stress-strain curve. $f_f - f_c$, f_n and C are parameters closely connected with the SE, which will be calibrated on the basis of the load-displacement relationships of the tensile tests in which void damage is dominated. According to Fu and Chan [13] and Furushima et al. [14], when the grain size of sheet metal is large, the fracture meachnism may be changed from void damage to single crystal deformation. The transition range of t/d is about 2 to 5. Therefore, the coarse grain size $d = 110.1\mu m$ should not be involved in calibration of void damage constants to avoid the possible interference of shear damage, and the experimental mechanical responses of the dog-bone tensile tests with small and medium grain size and sheet-0° tensile tests with medium grain size were employed in this procedure. The final results are shown in Table 2. As presented in Fig. 8, the simulation curves obtained with the above-calibrated parameters are almost the same as the experimental results in terms of the load level, ultimate fracture displacement, and the shape of the load-displacement responses, which proves the availability of the model and calibrated parameters. The acceptable error of load level mainly comes from the differences of flow stress calibrated by the combined constitutive model. Furthermore, the GTN model by Xu et al. [16] and the proposed GTN model with shear damage parameters determined later both predict the same results, indicating that the proposed model in this work is also valid when void damage is dominant in tensile tests.

Finally, shear damage parameters are calibrated by a sheet-90° test. As shown in Fig. 9, the simulated curves obtained with diverse ε_f^s and n are in comparison to the experimental curves. A larger ε_f^s will result in a delayed failure initiation, while a larger n will lead to a more sudden drop of load when the ε_p approaches to ε_f^s. Finally, $\varepsilon_f^s = 0.85$and $n = 2$ gives the most consistent results with the experimental results and thus are used as the calibrated shear damage parameters.

3. Results and discussion

3.1. Numerical results

As demonstrated in Fig. 10, the experimental load-displacement relationships and the corresponding simulation results are compared. Obviously, if there is no consideration of shear damage, the predictions of displacement at fracture by the modified GTN model proposed by Xu et al. [16] will deviate greatly from the experimental results, especially for sheet-90° test and sheet-45° tests with the medium and large grain sizes, which indicates the necessity of considering shear damage in fracture prediction under low stress triaxiality and shear-dominated conditions. Furthermore, when the shear damage is involved in the shear damage model introduced by Zhou et al. [21] but its SE is not considered, there are still obvious differences between the numerical and the experimental results when d is 45.07 μm and 110.1 μm. Therefore, the SE of shear damage should be characterized by the introduced size-related parameter. Besides, the void damage of sheet-45° is set as low values when the grain size is 45.07 μm and 110.1 μm because in these situations shear damage should be dominated. Finally, when both the shear damage and its SE are considered in the introduced combined model, the simulation results of all the tests with diverse d all have a good agreement with the experiments. The load shape and downtrend of the simulated curves calculated with the proposed model are much closer to the experimental curves than that calculated with the modified GTN model or the shear damage model, and more importantly, the prediction accuracy of displacement at fracture improves a lot. Therefore, the availability of the proposed model is proved.

The prediction error of displacement at fracture is also calculated and shown in Fig. 11. It is demonstrated that the prediction accuracy of the proposed model improves a lot than the modified GTN model and the shear GTN model. For most of the cases, the error between the prediction result based on the proposed model and the experimental result of is less than 5%. The root mean squared error $E_a = \sqrt{\sum_{i=1}^{n} e_i^2 / n}$ between the experiments and the results obtained with the modified GTN model, shear damage model and proposed model are 24.93%, 8.85%, 2.18%, respectively, which indicates the validity of the proposed model in different stress states and grain sizes.

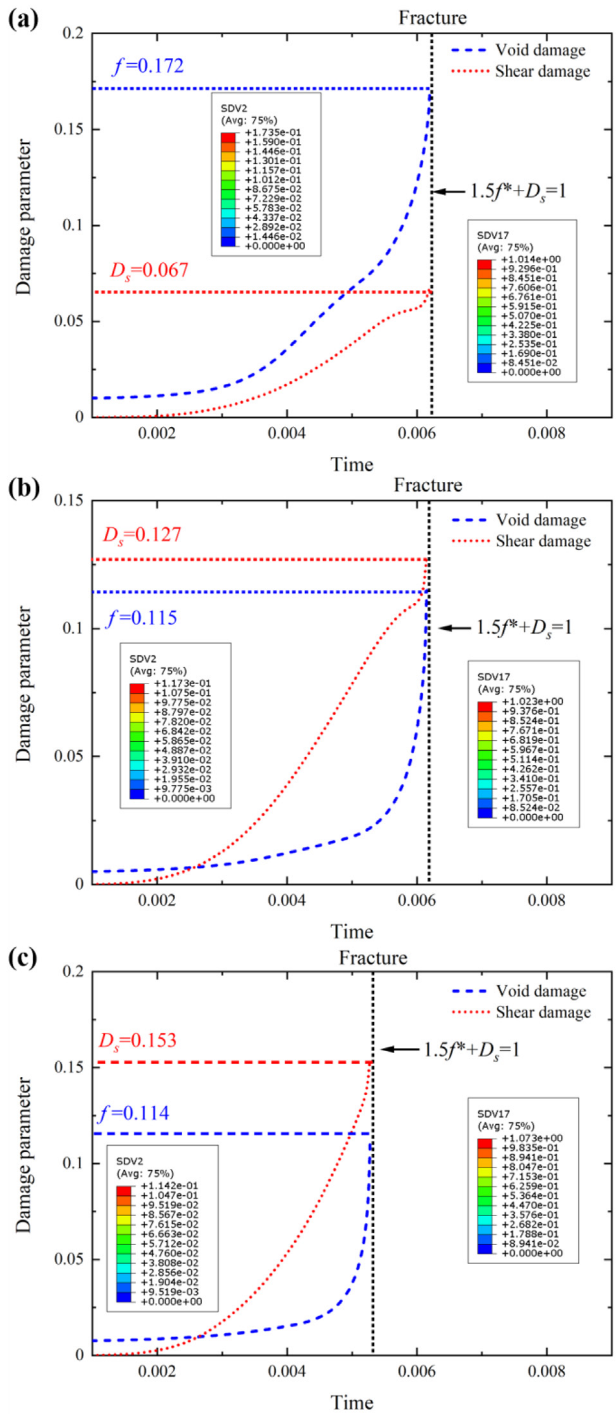

Fig. 15. The evolution of damage parameters of sheet-45° during deformation process. (a) 12.2 μm, (b) 45.07 μm, and (c) 110.1 μm.

3.2. Relationship between fracture mechanism and parameters

Li et al. [31] established and articulated the relationship panorama of the ductile fracture criteria, deformation modes and fracture mechanisms in macro-scale, and suggested the prediction accuracy of the DFC relies on whether or not several factors are considered, including stress triaxiality T and the Lode parameter η. There also exists a relation between the fracture mechanism and these parameters in the simulation results in the present work. Simulation results when the grain size of 12.2 μm are analyzed as follows. In view of the dog-bone tensile test, void damage is dominant. It is indicated in Fig. 12 that the stress triaxiality almost stays with 0.333 prior to the fracture and the Lode angle parameter is nearly unity, so the weight function is almost zero, which leads to the shear damage D_S almost negligible. Stress triaxiality of sheet-0° is even bigger, and the Lode parameter is similar to that of the dog-bone sheet, leading to a void-dominated damage similar to the dog-bone sheet. In contrast, the sheet-90° experiences a shear-dominated fracture when stress triaxiality changes from 0 to 0.2 during the deformation process and the Lode parameter is much smaller, indicating a shear-dominated stress state. When it comes to sheet-45°, there is a mixed fracture mode. The stress triaxiality is between 0 and 0.333, and the Lode parameter changes from 0.4 to 0.7.

Average stress triaxiality, Lode parameter and weight function of fracture initiation point are calculated and shown in Fig. 13. When the stress state changes from sheet-90° to sheet-0° over sheet-45° and dog-bone sheet, both T and ηincrease, and thus the weight function decreases and shear damage decreases, which is consistent with the phenomenon that with the increase of stress state, the void damage increases and become the dominant fracture mechanism. Therefore, the weight function and the law of shear damage evolution are both verified basically.

SEM photography also illustrates that different stress states will induce different fracture mechanisms. Fig. 14 shows the SEM fractography of various specimens with the grain size of 12.2 μm. It can be seen that in the fracture section of sheet-0°, there are many flat dimples at GB or inclusions. The reason is that they are barriers to dislocation motion and will result in stress concentration [13]. It means that a flat-dimple necking mechanism dominates at $T = 0.33$ and $\eta = 0.99$ for the dog-bone specimen. In the fracture surface of sheet-90°, shear dimples are observed and it is revealed that an inter-void shearing mechanism dominates at$T = 0.09$ and $\eta = 0.37$ for sheet-90°. When it comes to sheet-45° with $T = 0.18$ and $\eta = 0.61$, there is a mixed flat and shear dimple pattern and a combined tension-shear fracture mode occurs. It is considered that under the conditions of high and low stress triaxiality, the inter-void necking mechanism and the inter-void shearing mechanism is dominant, respectively [32]. Thus, lower stress triaxiality of specimens indicates shear-dominated fracture, and higher stress triaxiality indicates the void-dominated fracture.

3.3. SE on fracture mechanisms

The evolution of void damage and shear damage is obtained by solution-dependent state variables (SDV) in ABAQUS user subroutine, and the results of sheet-45° specimens are presented in Fig. 15 as the typical cases of the combined tensile-shear deformation conditions. During the deformation process, the two damage parameters f and D_S are all increased and the two fracture mechanisms compete with each other. When the total damage parameter D reaches 1, the final fracture occurs. When the fracture of specimen with the grain size of 12.2 μm occurs, the void damage parameter f is 0.172 and the shear damage parameter D_S is about 0.067, which reveals that a mixed mechanism fracture occurs and the void damage contributes more, leading to the fracture caused mainly by volumetric damage. When the grain size is 45.07 μm, the shear damage parameter D_S is 0.127 and the void damage parameter f is 0.115 when fracture initiates. Therefore, it is suggested that there is still a mixed fracture mechanism but as the grain size is larger, the fracture becomes shear-dominated. Moreover, the damage mechanism remains the same when the grain size is 110.1 μm. The shear damage parameter D_S is 0.153 and the void damage parameter f is 0.114, indicating that the fracture is also shear-dominated but the shear damage contributes more.

The contribution of the two damage mechanisms can be calculated by the ratio between the two damage parameters f and D_S. Other cases of sheet-0° test and the dog-bone sheet tests are also analyzed similarly, and the obtained data of the two damage contributions in different cases is calculated and represented in Fig. 16. When d is 12.2 μm, all

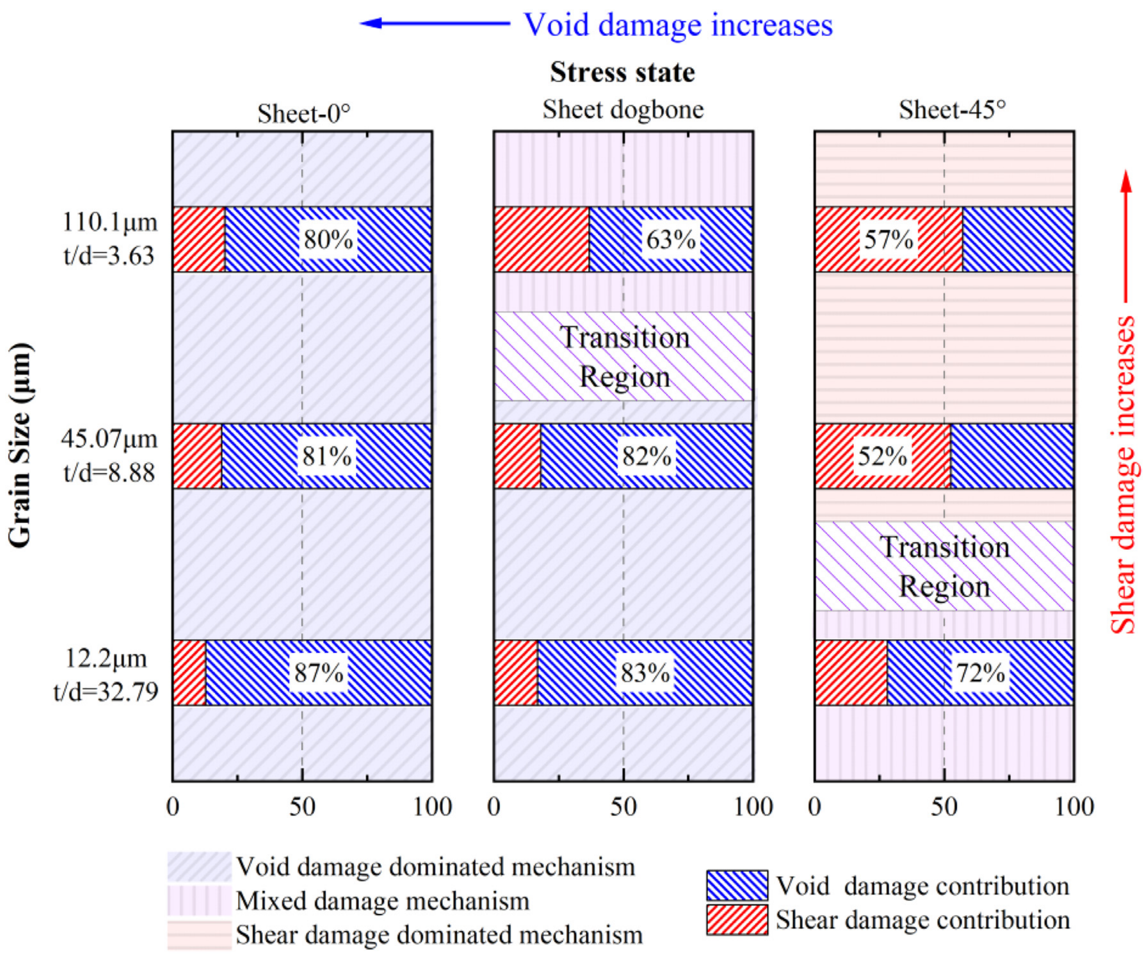

Fig. 16. The contribution of two fracture mechanisms obtained with the damage parameters in the proposed model.

the fracture of the dog-bone sheet, sheet-0° and sheet-45° are dominated by void damage. Even in the mixed fracture mechanism of sheet-45°, the proportion of void damage is nearly 72%, which contributes most of the fracture damage. The only case where the shear damage is dominated is the sheet-90° with fine grain and the shear damage contributes most of the total damage. With the increasing grain size, shear damage contributes more and more. When the grain size is 45.07 μm, the fracture of the dog-bone sheet, sheet-0° are still dominated by void damage and the shear damage contribution is only increased a bit, a negligible amount. The contribution of void damage is more than 80% in these cases, which indicates that the fracture is mainly induced by void damage. However, the contribution of shear damage in sheet-45° with the grain size of 45.07 μm is about 52% and slightly larger than the contribution of void damage, which indicates that the fracture mechanism changes from void-dominated to shear-dominated when t/d is decreased from 30 to 10. When the grain size is increased to 110.1 μm, the results are similar for both sheet-0° and sheet 45° and the slight difference is that shear damage accounts for a greater proportion. However, the fracture mechanism of dog-bone sheet changes to the mixed fracture mechanism with 37% contribution of shear damage. The considerable shear damage contribution may be caused by through-thickness shear bands for the coarsened grains, which is consistent with the results obtained by Zhang et al. [33]. Similarly, Fu and Chan [13] and Furushima et al. [14] also suggested the transition of fracture mechanism when grain size is increased to the same order of magnitude as the sheet thickness. The transition range of t/d from void-dominated fracture to mixed damage fracture predicted based on the proposed model is about 4 to 8, which agrees with experiment results by Furushima et al. [14] ($t/d \approx 3$~5) and crystal plasticity simulation results by Zhang et al. [33] ($t/d = 6$). Therefore, it could be concluded that with the grain size increases, shear damage increases and the dominant degree of shear fracture mechanism is increasing gradually. In contrast, with increasing$T$, the contribution of volumetric damage increases and the fracture mechanism is more dominated by the void damage as discussed in the section above.

All the results simulated by the proposed model are in consistent with the SEM fractography results. The fractured morphologies of sheet-45° samples are demonstrated in Fig. 17. When d is 12.2 μm, the mixed flat and shear dimples can be observed and there are more flat dimples, which agrees to the proportion analysis of volumetric damage and shear damage parameters. When the grain size is about 45.07 μm, there are mainly mixed flat and shear dimples in the fracture section and almost no void dimple is observed. Shear dimples and shear-dominated fracture are observed when the grain size is 110.1 μm, which is in consistent with the above quantitative analysis of the ratio between the two damage parameters in the proposed model. As shown in the SEM fractography, with increasing d, the number of voids is decreased. The distribution of voids is more uneven and the large and deep dimples exist in localization deformation. Therefore, it can be concluded that shear damage will dominate to a growing degree when the number of grains in the deformation area is sufficiently small in the thickness direction.

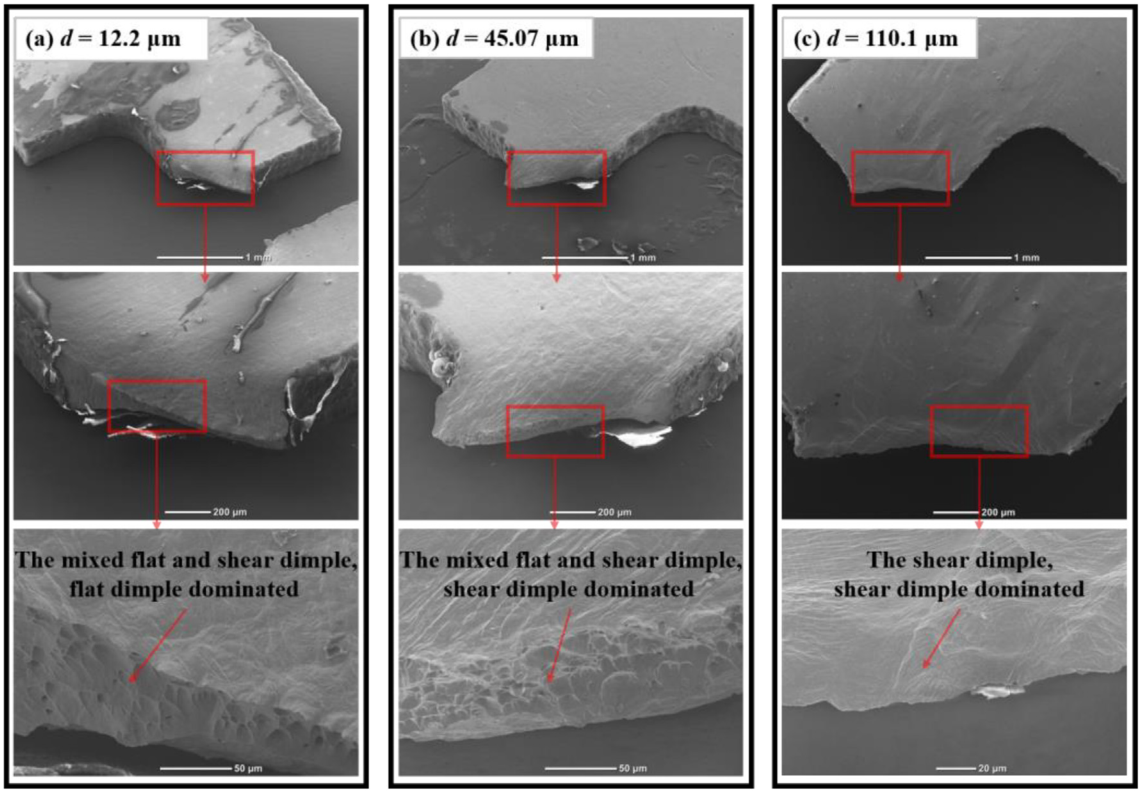

Fig. 17. SEM fractography of sheet-45° specimens with various grain sizes.

4. Conclusions

A combined GTN model, which takes both shear damage and size effect into consideration, is proposed, implemented and verified via a series of sheet tension tests and the comparison of finite element simulation and experimental results. The following concluding remarks are drawn based on these researches:

1. Upon a two-step calibration of the void and shear damage parameters, the proposed combined GTN model with consideration of shear damage and size effect could characterize damage response and fracture behavior well under the conditions of both low and high stress triaxiality, which improves the prediction accuracy of micro-scaled ductile fracture greatly with a 2.21% root mean squared error of the precited fracture displacement.
2. Shear damage is an important reason for micro-scaled ductile fracture and must be taken into consideration under low stress triaxiality conditions. Two independent damage parameters can be used in the combined GTN model to measure volumetric and shear damage separately and quantitatively, and the shear damage can be calculated in a phenomenological way with a weight function of Lode parameter.
3. Size effect has a great influence on micro-scaled plastic deformation and fracture behavior. The combined constitutive model is able to represent the size effect on flow stress of materials. The void damage is influenced by size effect on the void nucleation and coalescence, while the size effect on shear damage could be characterized by a size-related parameter.
4. Two fracture mechanisms of metallic material exist in different stress conditions. With the increase of stress triaxiality and Lode parameter, stress state changes and the dominated fracture mechanism is also changed from shear damage to void damage.
5. Size effect also affects the deformation of metallic materials and the mechanism of ductile fracture. With the increasing grain size, shear damage contributes more and the fracture mechanism becomes more shear-dominated, which is verified by not only the SEM metallography, but also the quantitatively numerical investigation of the damage variables in the proposed model. For dog-bone sheet, the transition range of t/d from void-dominated to mixed mechanism is about 4 to 8, while for sheet-45°, the transition range of t/d from mixed to shear-dominated mechanism is about 10 to 30.

Data availability

Representative samples of the research data are given in the figures and tables. Other datasets generated and/or analyzed during this study are not publicly available due to their large size but are available from the corresponding author upon reasonable request.

Declaration of Competing Interest

The authors declare that they have no known competing financial interests or personal relationships that could have appeared to influence the work reported in this paper.

Acknowledgements

The authors gratefully acknowledge funding supported by the Fundamental Research Funds of Shandong University, the Young Scholars Program of Shandong University, the Shenzhen Science and Technology Program (JCYJ20170818104529523), the China Postdoctoral Science Foundation funded project (2018 M632672), Shandong Provincial Natural Science Foundation (ZR2019BEE062), Natural Science Foundation of Jiangsu Province (BK20190202), National Natural Science Foundation of China (Grant No. 1705333, 51835011, 51575465), the Natural Science Foundation of Guangdong Province (Grant No. 2017A030310352).

References

[1] M.W. Fu, J.L. Wang, A.M. Korsunsky, A review of geometrical and microstructural size effects in micro-scale deformation processing of metallic alloy components, Int. J. Mach. Tool Manu. 109 (2016) 94–125, https://doi.org/10.1016/j.ijmachtools.2016.07.006.

[2] W. Yun, D. Peilong, X. Zhenying, Y. Hua, W. Jiangping, W. Jingjing, A constitutive model for thin sheet metal in micro-forming considering first order size effects, Mater. Des. 31 (2) (2010) 1010–1014, https://doi.org/10.1016/j.matdes.2009.07.037.

[3] L. Peng, X. Lai, H.-J. Lee, J.-H. Song, J. Ni, Friction behavior modeling and analysis in micro/meso scale metal forming process, Mater. Des. 31 (4) (2010) 1953–1961, https://doi.org/10.1016/j.matdes.2009.10.040.

[4] X.F. Tang, S.Q. Shi, M.W. Fu, Interactive effect of grain size and crystal structure on deformation behavior in progressive micro-scaled deformation of metallic materials, Int. J. Mach. Tool Manu. 148 (2020) 103473, https://doi.org/10.1016/j.ijmachtools.2019.103473.

[5] B. Meng, M.W. Fu, Size effect on deformation behavior and ductile fracture in microforming of pure copper sheets considering free surface roughening, Mater. Des. 83 (2015) 400–412, https://doi.org/10.1016/j.matdes.2015.06.067.

[6] J.W. Yoon, Metal forming - challenges in constitutive and fracture modeling, Int. J. Plast. 75 (2015) 1, https://doi.org/10.1016/j.ijplas.2015.09.012.

[7] A.L. Gurson, Continuum theory of ductile rupture by void nucleation and growth: part I—yield criteria and flow rules for porous ductile media, J. Eng. Technol. 99 (1) (1977) 2–15, https://doi.org/10.1115/1.3443401.

[8] V. Tvergaard, A. Needleman, Analysis of the cup-cone fracture in a round tensile bar, Acta Metall. 32 (1) (1984) 157–169, https://doi.org/10.1016/0001-6160(84)90213-X.

[9] P.F. Thomason, A three-dimensional model for ductile fracture by the growth and coalescence of microvoids, Acta Metall. 33 (6) (1985) 1087–1095, https://doi.org/10.1016/0001-6160(85)90202-0.

[10] Z.L. Zhang, C. Thaulow, J. Odegard, A complete Gurson model approach for ductile fracture, Eng. Fract. Mech. 67 (2) (2000) 155–168, https://doi.org/10.1016/S0013-7944(00)00055-2.

[11] L. Peng, F. Liu, J. Ni, X. Lai, Size effects in thin sheet metal forming and its elastic–plastic constitutive model, Mater. Des. 28 (5) (2007) 1731–1736, https://doi.org/10.1016/j.matdes.2006.02.011.

[12] F. Vollertsen, Z. Hu, Analysis of punch velocity dependent process window in micro deep drawing, Prod. Eng. 4 (6) (2010) 553–559, https://doi.org/10.1007/s11740-010-0241-6.

[13] M.W. Fu, W.L. Chan, Geometry and grain size effects on the fracture behavior of sheet metal in micro-scale plastic deformation, Mater. Des. 32 (10) (2011) 4738–4746, https://doi.org/10.1016/J.Matdes.2011.06.039.

[14] T. Furushima, H. Tsunezaki, K.-i. Manabe, S. Alexsandrov, Ductile fracture and free surface roughening behaviors of pure copper foils for micro/meso-scale forming, Int. J. Mach. Tool Manu. 76 (2014) 34–48, https://doi.org/10.1016/j.ijmachtools.2013.10.001.

[15] J.Q. Ran, M.W. Fu, A hybrid model for analysis of ductile fracture in micro-scaled plastic deformation of multiphase alloys, Int. J. Plast. 61 (10) (2014) 1–16, https://doi.org/10.1016/j.ijplas.2013.11.006.

[16] Z.T. Xu, L.F. Peng, M.W. Fu, X.M. Lai, Size effect affected formability of sheet metals in micro/meso scale plastic deformation: experiment and modeling, Int. J. Plast. 68 (2015) 34–54, https://doi.org/10.1016/j.ijplas.2014.11.002.

[17] L. Xue, Constitutive modeling of void shearing effect in ductile fracture of porous materials, Eng. Fract. Mech. 75 (11) (2008) 3343–3366, https://doi.org/10.1016/j.engfracmech.2007.07.022.

[18] K. Nahshon, J.W. Hutchinson, Modification of the Gurson model for shear failure, Eur. J. Mech. Solid. 27 (1) (2008) 1–17, https://doi.org/10.1016/j.euromechso1.2007.08.002.

[19] K.L. Nielsen, V. Tvergaard, Ductile shear failure or plug failure of spot welds modelled by modified Gurson model, Eng. Fract. Mech. 77 (7) (2010) 1031–1047, https://doi.org/10.1016/j.engfracmech.2010.02.031.

[20] M. Achouri, G. Germain, P. Dal Santo, D. Saidane, Experimental characterization and numerical modeling of micromechanical damage under different stress states, Mater. Des. 50 (2013) 207–222, https://doi.org/10.1016/j.matdes.2013.02.075.

[21] J. Zhou, X. Gao, J.C. Sobotka, B.A. Webler, B.V. Cockeram, On the extension of the Gurson-type porous plasticity models for prediction of ductile fracture under shear-dominated conditions, Int. J. Solids Struct. 51 (18) (2014) 3273–3291, https://doi.org/10.1016/j.ijsolstr.2014.05.028.

[22] J. Lemaitre, A continuous damage mechanics model for ductile fracture, J. Eng. Technol. 107 (1985) 83, https://doi.org/10.1115/1.3225775.

[23] J.L. Wang, M.W. Fu, S.Q. Shi, Influences of size effect and stress condition on ductile fracture behavior in micro-scaled plastic deformation, Mater. Des. 131 (2017) 69–80, https://doi.org/10.1016/j.matdes.2017.06.003.

[24] W.T. Li, H. Li, M.W. Fu, Interactive effect of stress state and grain size on fracture behaviours of copper in micro-scaled plastic deformation, Int. J. Plast. 114 (2019) 126–143, https://doi.org/10.1016/j.ijplas.2018.10.013.

[25] X. Lai, L. Peng, P. Hu, S. Lan, J. Ni, Material behavior modelling in micro/meso-scale forming process with considering size/scale effects, Comput. Mater. Sci. 43 (4) (2008) 1003–1009, https://doi.org/10.1016/j.commatsci.2008.02.017.

[26] L. Peng, X. Lai, H.-J. Lee, J.-H. Song, J. Ni, Analysis of micro/mesoscale sheet forming process with uniform size dependent material constitutive model, Mat. Sci. Eng. Struct. 526 (1–2) (2009) 93–99, https://doi.org/10.1016/j.msea.2009.06.061.

[27] J.Q. Zhou, Z.H. Li, R.T. Zhu, Y.L. Li, Z.Z. Zhang, A mixtures-based model for the grain size dependent mechanical behavior of nanocrystalline materials, J. Mater. Process. Technol. 197 (1–3) (2008) 325–336, https://doi.org/10.1016/j.jmatprotec.2007.06.047.

[28] C. Chu, A. Needleman, Void nucleation effects in biaxially stretched sheets, J. Eng. Technol. 102 (3) (1980) 249–256, https://doi.org/10.1115/1.3224807.

[29] A.A. Benzerga, J. Besson, A. Pineau, Coalescence-controlled anisotropic ductile fracture, J. Eng. Technol. 121 (2) (1999) 221–229, https://doi.org/10.1115/1.2812369.

[30] J. Besson, Damage of ductile materials deforming under multiple plastic or viscoplastic mechanisms, Int. J. Plast. 25 (11) (2009) 2204–2221, https://doi.org/10.1016/j.ijplas.2009.03.001.

[31] H. Li, M.W. Fu, J. Lu, H. Yang, Ductile fracture: experiments and computations, Int. J. Plast. 27 (2) (2011) 147–180, https://doi.org/10.1016/j.ijplas.2010.04.001.

[32] I. Barsoum, J. Faleskog, Rupture mechanisms in combined tension and shear - experiments, Int. J. Solids Struct. 44 (6) (2007) 1768–1786, https://doi.org/10.1016/j.ijsolstr.2006.09.031.

[33] H. Zhang, J. Liu, D. Sui, Z. Cui, M.W. Fu, Study of microstructural grain and geometric size effects on plastic heterogeneities at grain-level by using crystal plasticity modeling with high-fidelity representative microstructures, Int. J. Plast. 100 (2018) 69–89, https://doi.org/10.1016/j.ijplas.2017.09.011.